

# The MSX/UVISI Stellar Occultation Experiments: Proof-of-Concept Demonstration of a New Approach to Remote Sensing of Earth's Atmosphere

Ronald J. Vervack Jr., Jeng-Hwa Yee, William H. Swartz,  
Robert DeMajistre, and Larry J. Paxton

A primary means of monitoring the atmosphere on a global scale is remote sensing of Earth from space, and occultation methods based on observing changes in a star's spectrum as it sets through the atmosphere have proven valuable in this endeavor. Two occultation techniques—focused respectively on atmospheric extinction and refraction—have been treated separately historically, but the combination of the two offers the possibility of higher accuracy, greater altitude coverage, and simultaneous measurement of primary and trace gases, both of which are important in the chemical balance of the atmosphere. Using data from the Ultraviolet and Visible Imagers and Spectrographic Imagers (UVISI) on the Midcourse Space Experiment (MSX) satellite, we have developed a combined extinctive/refractive stellar occultation technique that relates the changes in measured stellar intensity to the height-dependent density profiles of atmospheric constituents and have demonstrated its viability for retrieving both primary and trace gases through the analysis of approximately 200 stellar occultations. This self-calibrating technique is broadly applicable and suitable for measurement of gases that are otherwise difficult to quantify on a global basis. In this article, we summarize the development of the technique, its validation through comparison to other measurements, and its application to the study of Earth's overall atmosphere and lower atmosphere in particular.

## INTRODUCTION

The Earth's atmospheric composition, temperature, and ability to cleanse itself chemically have coevolved with biological life on geological timescales.<sup>1</sup> On much

shorter timescales, however, anthropogenic activities have effected changes in the atmosphere. Much of the observed change is associated with minor atmo-

spheric constituents, referred to as trace gases, and their impact on atmospheric chemistry. Although many of the Earth's trace gases exist naturally, the rapid rise in the concentrations of both native and nonnative gases and their observed effects on the atmosphere's chemical balance over the past 150 years or so is coincident with industrialization and the advent of modern agricultural practices.<sup>2</sup> Whereas studies assessing the long-term consequences of these changes are ongoing, a significant obstacle is often a lack of regular, global measurements of the concentrations of these trace gases in the atmosphere, particularly in the lower atmosphere (less than 50 km altitude) where their concentrations and effects are most significant. Measurement of emission spectra from atoms and molecules is often used to probe atmospheric densities, but many of the important trace gases in the atmosphere emit such radiation weakly or not at all, or their emission signatures are convolved with stronger emission from other atoms or molecules and cannot be separated. As such, these trace gases can only be detected through *in situ* sampling or via remote observation of their attenuation or scattering of light.

Stellar occultation is one of the most promising techniques to meet the needs of atmospheric scientists, policy makers, and enforcement agencies tasked with understanding and regulating man-made contributions to the trace gas atmospheric budget. Occultation techniques have been used for many years to study the atmospheres of Earth, other planets, and their satellites. Because these techniques are generally based on relative measurements (i.e., compared to measurements in the absence of the occulting atmosphere), they tend to be less sensitive to

instrument degradation and changes in calibration than other remote sensing methods. Although these techniques are easy to implement in principle, technical hurdles exist. As these challenges have been overcome, occultation techniques have proven to be an excellent means of exploring the overall structure of both terrestrial and planetary atmospheres.

Using occultation methods to probe Earth's lower atmosphere is complicated by the effects of both refraction and extinction as light passes through the densest part of the atmosphere. To demonstrate a new approach to this challenge, we took advantage of the Ultraviolet and Visible Imagers and Spectrographic Imagers (UVISI) suite of instruments onboard the Midcourse Space Experiment (MSX) spacecraft to conduct stellar occultation experiments in which we combined techniques suited to measuring refraction and extinction independently into a single, self-consistent occultation method that leverages the benefits of both techniques. This demonstration led to the development of an instrument concept suitable for flight on a small space platform.

The potential measurement capabilities of this combined stellar occultation technique are illustrated in Fig. 1. The left panel shows the retrievable altitude ranges for several gas and aerosol constituents in the terrestrial atmosphere that can be measured over far-UV to visible wavelengths, whereas the right panel shows the altitude ranges for gases that can be measured in the near-IR. These altitude ranges are derived from an analysis of the extinction spectra for the various species (a term commonly applied to atmospheric constituents) and the

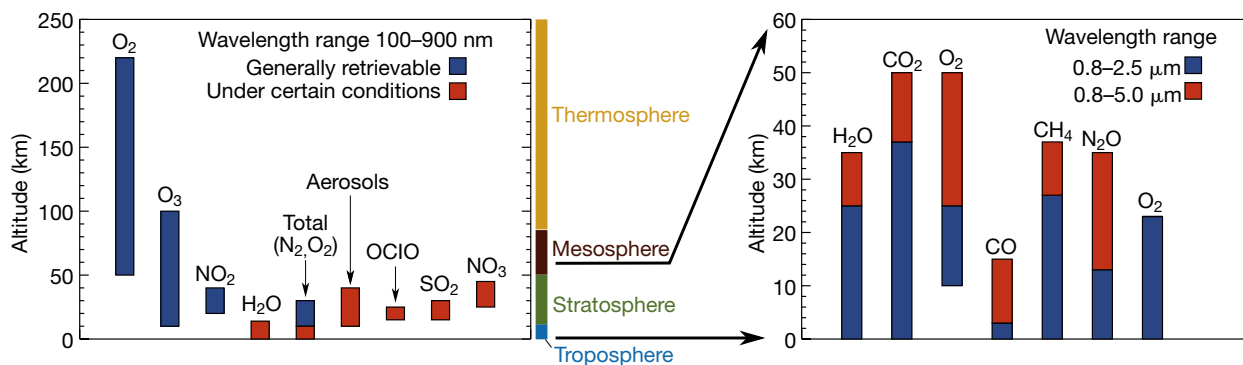


**Figure 1.** Illustration of the measurement capabilities of the combined occultation technique. The left panel shows the retrievable altitude ranges for several species in the terrestrial atmosphere that can be measured over the wavelength range of 100–900 nm. The blue bars represent ranges that are generally measurable under all conditions, whereas the red bars represent ranges that vary depending on the atmospheric conditions (e.g., night/day, presence of high-altitude clouds) and the target star involved (e.g., spectral type, magnitude). Colored bars along the right y axis denote the altitude ranges of various atmospheric regions. The right panel shows the retrievable altitude ranges for several terrestrial species that can be measured if coverage is extended into near-IR wavelengths: 0.8–2.5 μm (blue bars) or 0.8–5.0 μm (blue+red bars). In both panels, the actual lower limits of the altitude ranges are determined by cloud-top heights at the time of the occultation; the limits shown are for clear skies. Note that the upper limits on CO<sub>2</sub> and O<sub>3</sub> in the right panel are truncated to 50 km to allow the panel to focus on the lower altitudes.

capabilities of an instrument optimized for their measurement, particularly in the lower atmosphere where refraction effects must be accounted for in extinctive occultation observations. We will explore the basis for these altitude ranges as we discuss our proof-of-concept measurements with MSX/UVISI throughout this article.

Owing to the low altitudes that must be reached before near-IR extinction is significant, an occultation technique combining extinctive and refractive measurements is both ideal and necessary: ideal because measuring the bulk atmosphere and the trace species simultaneously provides a complete picture of the atmosphere, and necessary because refraction effects are intertwined with the extinction and must be separated. Several hundred stars are bright enough and of an appropriate spectral class for far-UV and visible wavelength occultations. As wavelength increases, there are fewer stars of sufficient brightness or spectral class; approxi-

mately 50 remain suitable out to  $2.5\ \mu\text{m}$ , and only 10–20 are viable out to  $5\ \mu\text{m}$ . We can, however, take advantage of the slow motion of Earth relative to the background stars—it takes many days for Earth to progress in its orbit such that a given star is no longer available as an occultation source. Thus, a given star may be used many times when it is observable, and the additional spectral coverage out to near-IR wavelengths is worth consideration given the extended range of altitudes and species it enables.

We first give a brief historical perspective on stellar occultation techniques to set the stage for a description of the MSX/UVISI stellar occultation experiments. We then highlight the success of these proof-of-concept measurements and explore the future possibilities for the combined stellar occultation technique as a means of probing Earth's atmosphere.

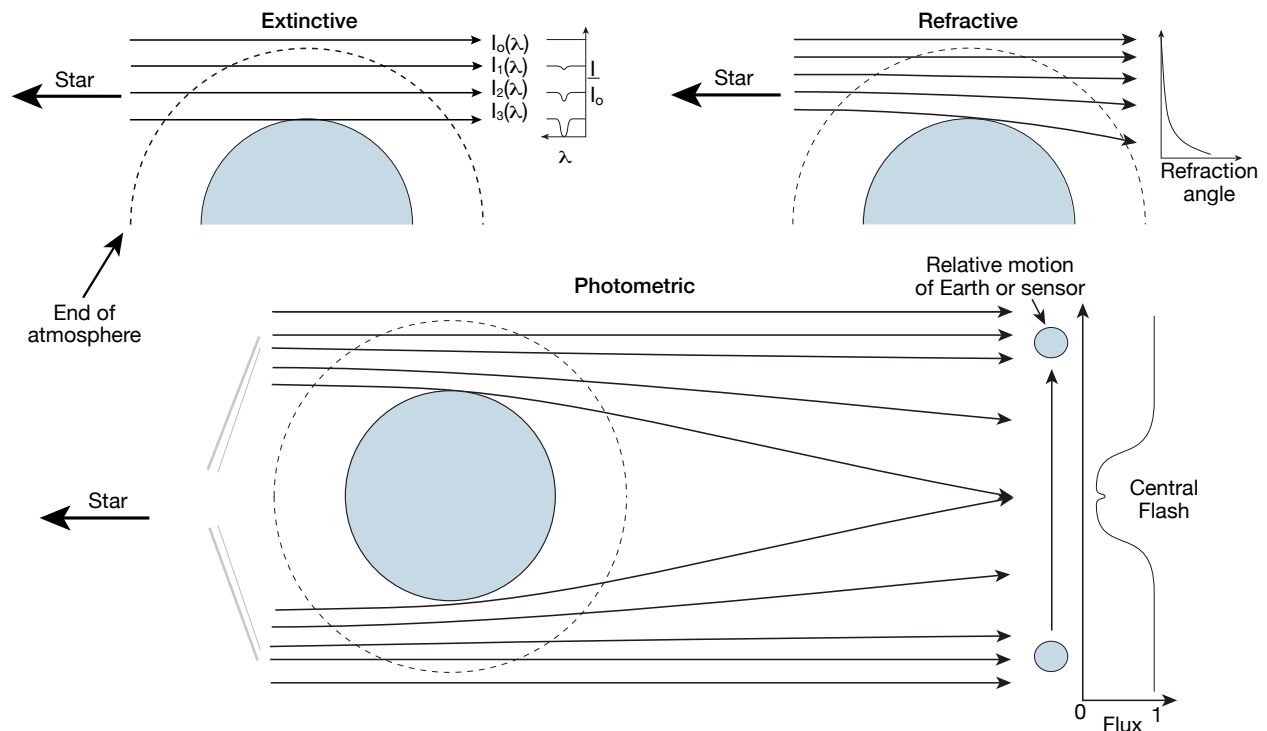


**Figure 2.** Geometric illustrations of the principles of various stellar occultation methods. In all three panels, the star is to the left and far enough away that the incoming rays can be considered parallel. The upper left panel shows the geometry of an extinctive occultation, in which the flux  $I_0(\lambda)$  from a star is progressively attenuated as the line of sight to the star moves deeper into the atmosphere. The ratio of the measured flux  $I$  at each point to the stellar flux is  $I/I_0$ , known as the atmospheric (or stellar) transmission. Transmission values run from 0 (full extinction) to 1 (no extinction) and are a function of wavelength because the extinction by the atmosphere depends on the wavelength. The upper right panel shows the geometry of a refractive occultation, in which the angle between the observed ray and the unrefracted ray (the incoming stellar ray) is measured. The deeper in the atmosphere the line of sight penetrates, the larger the measured refraction angle will be. The lower panel shows the geometry of a photometric occultation, which is a variant on the refractive occultation. In this case, rather than measure the refraction angle of the star, the total flux from the star is measured. As the rays from the star diverge due to refraction, the relative flux measured at the sensor drops from a value of 1 outside the atmosphere to 0 when the star is blocked by the planet. This is because diverging rays fall outside the sensor field of view, and the greater the divergence, the less flux that is measured. The central flash often seen in the total flux is caused by the convergence of rays refracted around opposite sides of the planet even though the star itself is completely blocked.

## THE STELLAR OCCULTATION TECHNIQUE

Two general categories of occultations exist: extinctive and refractive. In both, radiation from a source is affected by physical processes in the atmosphere, and measurements of the outgoing radiation are used to infer atmospheric properties. In the following sections, we briefly describe the techniques that have evolved for these two types of occultations. Although the Sun, stars, and radio signals have all been used as the sources in occultations, we focus on stellar occultations for reasons that will be made apparent in the discussion.

### Extinctive Stellar Occultations

The principles of extinctive stellar occultations are similar to those of classical absorption spectroscopy. As shown in the upper left of Fig. 2, a star is used as the light source, a spectrometer serves as the detector, and the intervening atmosphere acts as the absorption cell. The spectrometer is most commonly mounted on a spacecraft but may also be on Earth's surface or on a balloon, in which case the effective absorption path is half that shown in the figure. Starlight passing through the atmosphere is attenuated because atmospheric constituents either absorb or scatter the incoming light. Although the physical process involved is different, the net effect of extinction by scattering (molecular/Rayleigh or aerosol/Mie scattering) is similar to that by absorption (i.e., scattering "out of the beam" reduces light intensity far more than scattering "into the beam" increases it); therefore, the term *extinction* as used here refers to any absorption or scattering process. As the line of sight to the star moves deeper into the atmo-

sphere, the light is progressively attenuated because the effective extinction path length increases. At the same time, changes in the densities of the species responsible for extinction along the path are recorded in the measured spectra. The ratio of an attenuated spectrum,  $I$ , to the unattenuated spectrum,  $I_0$ , is referred to as the atmospheric (or stellar) transmission and is the fraction of light that passes through the atmosphere as a function of wavelength. The minimum altitude to which a ray penetrates is referred to as the tangent point height or tangent point altitude of the measurement, or more simply as the tangent point. Note that in this article, we use *altitude* to refer to the actual altitudes relevant to atmospheric density profiles, whereas *tangent point altitude* or *height* is used to refer to the minimum altitude of an observation. The distinction is subtle but will be made clear as we discuss the observations.

Because the extinction cross sections of most species are wavelength dependent, spectral measurements of the transmission represent a "fingerprint" of the relevant species. Thus, they are diagnostic of the atmospheric composition, and densities of the species involved can be determined from the observed transmission spectra. Figure 3 illustrates the wavelength dependence of the altitude at which the density of several species results in a specific level of extinction, in this case the  $\tau = 0.1$  level. Extinction in the atmosphere is generally proportional to the function  $\exp(-\tau(\lambda))$ , where  $\lambda$  is the wavelength and  $\tau$  is referred to as the optical depth; thus,  $\tau = 1$  refers to the point in the atmosphere at which the total flux from a star at a given wavelength has decreased to  $1/e$  of its unattenuated value. Because the transmission is related to the optical depth, this figure is also illustrative

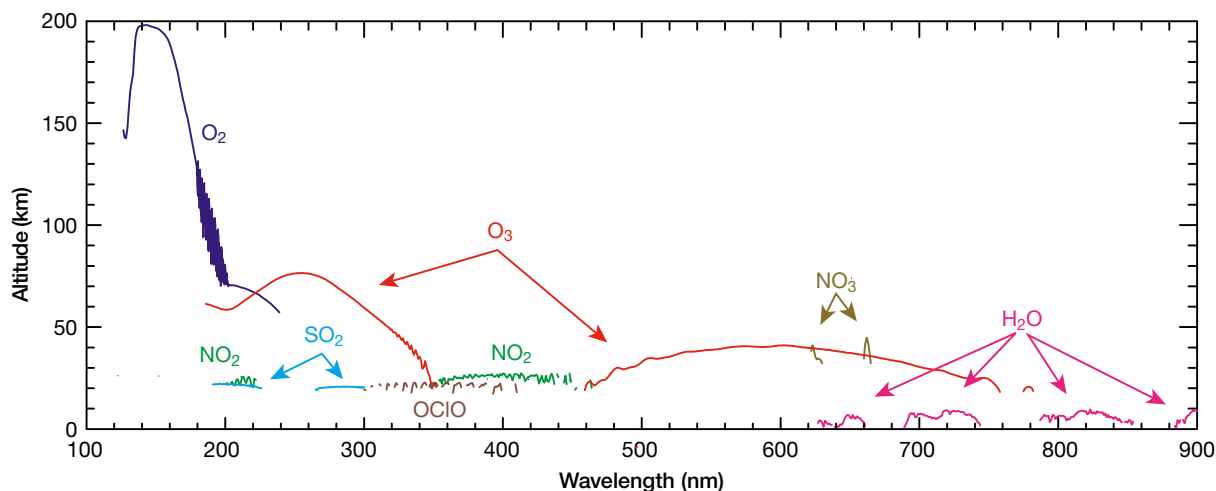


**Figure 3.** Altitudes at which the line-of-sight optical depth for several species in the terrestrial atmosphere reaches the  $\tau = 0.1$  level ( $\tau = 0.01$  for OCIO and  $\text{NO}_3$ ) as a function of wavelength. Because extinction is generally proportional to the function  $\exp(-\tau)$ , the  $\tau = 1$  level is that point in the atmosphere at which the total flux from a star at a given wavelength has decreased to  $1/e$  of its unattenuated value. Because the extinction character of different atmospheric species varies with wavelength, plots such as this are helpful in designing occultation instruments because they highlight where extinction is most likely and indicate the altitude ranges in the atmosphere that it is possible to probe (e.g., see Fig. 1).

of the range of altitudes over which the density profiles of such species may be inferred from transmission spectra. Extinction as a function of wavelength and altitude for the species in Fig. 3 and for other species form the basis of the altitude ranges illustrated in Fig 1. With a properly designed instrument, accurate retrievals can generally be carried out over transmissions ranging from 1 to 99% ( $\tau$  ranges of roughly 0.01–4.5).

The possibility of using stars as the source in an extinctive occultation observed by a space-based platform was first suggested by Hays and Roble.<sup>3</sup> The first stellar occultation measurements of the terrestrial atmosphere came a few years later when a spectrometer on the Orbiting Astronomical Observatory (OAO)-2 satellite was used to infer density profiles for molecular oxygen ( $O_2$ ) and ozone ( $O_3$ ) in the thermosphere and upper mesosphere.<sup>4–6</sup> Since OAO-2, extinctive stellar occultations have yielded densities for a number of species in Earth's atmosphere, including  $O_2$ ,  $O_3$ , NO,  $NO_2$ ,  $NO_3$ ,  $N_2O$ ,  $H_2$ ,  $CH_4$ , CO,  $H_2O$ , Cl, and OClO.<sup>7–10</sup> As mentioned above, because many of these species do not exhibit emission features that are directly indicative of their density, the stellar occultation technique provides a unique insight into atmospheric composition. The technique has also been a primary means of probing the atmospheres of the other planets and their satellites. The ultraviolet spectrometers on Voyagers 1 and 2 observed stellar occultations by the atmospheres of Jupiter, Saturn, Uranus, Triton, and Ganymede.<sup>11,12</sup>

### Refractive Stellar Occultations

Refractive stellar occultations occur because density gradients in the atmosphere lead to refraction, or bending, of the path of incoming starlight. This results in the light following curved paths through the atmosphere, which leads to differences between the star's true (geometric) and apparent (refracted) positions. Measurements of the degree to which the path of the incoming starlight is changed provide the bulk properties of the atmosphere (i.e., total density, pressure, temperature). Pannekoek<sup>13</sup> first realized the potential of refraction for studying planetary atmospheres, but roughly 50 years would pass before technology progressed to the point that useful observations could be made.

The primary refractive stellar occultation technique is the photometric approach (see the lower panel in Fig. 2), which involves visible-light observations of the occultation of stars by a planetary atmosphere using ground, aircraft, or space-based telescopes. This approach has been applied primarily to the study of the atmospheres of the other planets. As a star passes behind a planet, light rays passing through deeper regions of the atmosphere are refracted more than rays at higher altitudes. This results in a divergence of the incoming parallel light from the star. At the detector, the divergence appears as an atten-

uation of the light as a function of time (referred to as refractive attenuation) as more and more of the total flux from the star is refracted out of the field of view of the sensor. Photometric observations of this attenuation yield the so-called occultation light curve, which may be inverted to retrieve the atmospheric density, pressure, and temperature.

The first useful application of this technique was by Baum and Code,<sup>14</sup> who determined the mean molecular weight of Jupiter's atmosphere from an occultation of the star  $\sigma$  Arietis. Since then, numerous occultations of stars by other planets have been observed, and the technique has evolved into a powerful method for remotely probing planetary atmospheres. The literature is extensive; however, a representative sample may be found in Refs. 15–18. Summaries of the general methods and much of the early work are given in Refs. 19 and 20.

Often, these photometric occultations yield light curves that exhibit rapid fluctuations in intensity. These fluctuations are caused by a refractive phenomenon known as scintillation, which arises from small-scale variations in the density profile at points along the line of sight. Such variations may be caused by atmospheric turbulence or by the presence of atmospheric waves. When combined with models of such variations, measurements of the scintillation have proven useful in inferring the small-scale atmospheric structure.<sup>16</sup>

### Earth's Lower Atmosphere

Historically, extinctive stellar occultations have been applied to high altitudes for three reasons. First, the species involved (e.g.,  $O_2$  and  $O_3$  for Earth) have strong spectral signatures at UV wavelengths, which are completely absorbed by the atmosphere before the lower altitudes are reached. Second, the presence of atmospheric emissions (e.g., airglow) from other species that occur in the instrumental bandpass used in the occultation experiment leads to an additional source that competes with the stellar signal. Once the line of sight to the star has passed below the atmospheric level of such emission, which ranges in altitude depending on the wavelength and species involved, the emission is always present as a contaminating source. Separation of the stellar and emission sources is therefore necessary and can be complicated. Finally, there are no significant refractive effects at high altitudes, allowing a straightforward interpretation of the observed transmission.

Refractive stellar occultations have been limited almost exclusively to the study of other planets. The primary reason for this is that the long distances involved allow for a greater separation of the diverging rays and a more easily measured change in the stellar intensity. At the same time, the choice of visible wavelengths for these occultations generally excludes the need to consider extinction of the starlight within the atmosphere itself.

These extinctive and refractive methods, however, are complementary, and consideration of both processes would allow stellar occultation measurements to probe a larger altitude range more accurately than either one taken individually. In particular, the idea of using extinctive stellar occultations to probe Earth's lower atmosphere by considering the effects of refraction on the measurements was first proposed by Hays and Roble.<sup>3</sup> They favored stellar occultations over solar occultations, which have been the primary occultation method of studying Earth's lower atmosphere, for a number of reasons. Stellar occultations are not limited to the terminator and allow for hundreds of occultations per day with near-global coverage versus the 30 or so daily using solar occultations. Stellar occultations can also yield higher vertical resolution owing to the point nature of the source; the Sun subtends an angular range of half a degree, which corresponds to about 30 km in altitude. Solar occultations do yield higher signal-to-noise ratio observations owing to the intensity of the Sun relative to stars, and solar occultations are generally immune to the effects of atmospheric emissions because the Sun is so much brighter than the atmosphere. However, in the lower atmosphere where refraction is significant, stellar occultations have the advantage over solar occultations in that the refractive effects can be treated more easily for stars (as point sources) than for the Sun (as an extended source).

Although only a theoretical study, the Hays and Roble work demonstrated that the extinctive stellar occultation technique could be a powerful tool for remotely sensing Earth's atmosphere. However, the implementation requirements for this technique, especially in the lower atmosphere, are rather stringent. Because stars are often a relatively low-intensity source, the instrument has to have a high signal-to-noise ratio to allow occultations by moderately bright stars, thereby maximizing the number of available stars. A high-precision, two-axis system is needed to acquire and track the star as it sets through the atmosphere, including the apparent motion induced by refraction. To infer altitude profiles, multi-wavelength measurements at moderate to high spectral resolution are needed to separate the spectral signatures of the various atmospheric species. The presence of atmospheric emissions requires a hyperspectral imaging system with both spectral and spatial dimensions. Finally, to track the star even in the presence of refraction, the spacecraft, instrument, or both must have excellent stability and jitter compensation. Reducing this idea to practice had to wait until the MSX opportunity.

## MSX/UVISI STELLAR OCCULTATIONS

The MSX satellite—designed, built, and tested at the Johns Hopkins University Applied Physics Labo-

ratory (APL) for the Ballistic Missile Defense Organization—was launched into a 900-km, circular, near-Sun-synchronous orbit on April 24, 1996. As a three-axis stabilized spacecraft, MSX was capable of extraordinarily accurate and stable pointing. Inertial targets such as stars were observable with an absolute accuracy approaching  $\sim 100 \mu\text{rad}$  and a relative stability of  $\sim 10 \mu\text{rad}$  ( $1 \sigma$ ) over a time span of several minutes. The UVISI instrument package consisted of four visible and UV imagers (two narrow field-of-view and two wide field-of-view) and five spectrographic imagers (SPIMs) covering the wavelength range of 120–900 nm. All nine instruments were co-aligned within  $50 \mu\text{rad}$  along the long axis of the spacecraft and mounted on a common optical bench to maintain the co-alignment. Thorough descriptions of MSX and the UVISI instruments may be found in Refs. 21–23.

We took advantage of the capabilities of MSX and UVISI to test the suggestions of Hays and Roble<sup>3</sup> and thereby demonstrate the viability of using stellar occultations for the retrieval of atmospheric composition, particularly in the lower atmosphere. Although the MSX spacecraft and the UVISI suite of instruments were not specifically designed for stellar occultations, their combination fortuitously satisfied the stringent requirements necessary to conduct these experiments. Rather than simply use models or climatological information to treat the effects of refraction on the extinctive measurements, the MSX/UVISI experiments focused on a combined extinctive *and* refractive stellar occultation technique in which SPIMs were used to measure the wavelength-dependent atmospheric extinction of starlight while a co-aligned imager (IVN) was used to measure the atmospheric refraction along the same line of sight.

The key element in this new approach to stellar occultations was the direct measurement of the refraction angle of the star at visible wavelengths, as suggested by Jones et al.<sup>24</sup> Although simple in concept, this method of refraction angle measurement has previously been used in only a few, mostly serendipitous, instances.<sup>25,26</sup> The MSX/UVISI experiments represent the first systematic implementation of the technique. The refraction angles themselves are used to infer atmospheric refractivity and subsequently the bulk atmospheric density, pressure, and temperature. Although the temperature profiles determined from such measurements are unlikely to ever be as accurate as profiles derived from radio occultation methods such as those used in GPS/MET (Global Positioning System/Meteorology),<sup>27,28</sup> the advantage of this visible-light technique is that the refraction angles are measured simultaneously along the same line of sight as the extinction measurements.

By simultaneously measuring both refraction and extinction effects on the stellar spectrum, the extinction measurements were able to probe the atmospheric com-

position accurately at the low altitudes where refraction is significant. Measurements of refraction provided the actual light path through the atmosphere and the bulk atmospheric properties, both of which are necessary to determine extinction accurately in the refractive region of the lower atmosphere. More importantly, knowledge of the total density profile allowed the effects of Rayleigh scattering in the transmission spectra to be handled accurately. The simultaneous measurement of both constituent and total density profiles also allowed for direct calculation of volume mixing ratios, a key quantity that typically has to be inferred and is therefore subject to increased uncertainty.

The design of the MSX/UVISI stellar occultation experiments and the associated extinction and refraction retrieval algorithms are discussed in detail in a three-paper series.<sup>29–31</sup> A full discussion of the combined technique, the development of the retrieval algorithms, and a rigorous assessment of the uncertainties may be found in these papers. In this article, we present an overview of the technique and analysis methods along with a summary of several results that highlight the potential of the combined extinctive and refractive stellar occultation technique for studying Earth's atmosphere.

### Typical MSX/UVISI Occultation Event

The geometry of a typical MSX/UVISI stellar occultation event is shown in Fig. 4. The star was acquired at high tangent altitudes and the boresights of the UVISI instruments remained fixed on the star's inertial position during the entire occultation. The entrance slits to the five spectrographs were held vertical with respect to the horizon. Several hundred unattenuated  $I_0$  spectra were obtained at high altitudes before any atmospheric effects began. As the star set through the atmosphere, its spatial position in the spectrograph images was unchanged until refraction set in at altitudes below roughly 35 km, after which the image drifted vertically up the slit until it slowly disappeared from the field of view. For a star inertially fixed in the center of the slit, roughly  $0.5^\circ$  of motion due to refraction could be observed before the star's image reached the edge of the frames, corresponding to apparent tangent point altitudes of 7–8 km. As seen in path 5 of Fig. 4, the direct

line of sight to the star (dashed line) at that point actually had a tangent point altitude below the horizon. The tangent point altitude of the direct line is referred to as the geometric tangent point altitude and can be negative. When refraction is not important (i.e., above 35 km), the apparent and geometric tangent point altitudes are the same.

As illustrated in Fig. 4, airglow emissions are an issue. These first appear in the bottom edge of a spectrographic slit as it descends through the altitudes at which the emissions originate (e.g., the airglow layer). The peak in the emission layer signal will continue to move up the slit, eventually disappearing above the top edge. However, once the line of sight passes through the airglow layer, the stellar signal is superimposed on an ever-present background airglow signal. Because each spatial pixel covers a field of view of  $\sim 0.025^\circ$  (about 1.5 km projected onto the limb), the UVISI SPIMs are essentially used as large-aperture photometers ( $\sim 100 \text{ cm}^2$ ) with an effective field of view of  $0.1^\circ \times 0.025^\circ$ . With a maximum star setting rate of roughly  $0.07^\circ/\text{s}$  ( $\sim 3 \text{ km/s}$ ), the limb airglow emission at a given tangent point altitude is sampled for approximately 10 s. On the ground, this multiple sampling of the airglow allows us to “shift” the SPIM pixels spatially and co-add them in a manner similar to that used for a time-delay and integration system, thereby improving the signal-to-noise ratio of the observations and subsequent accuracy of the separation of the stellar and airglow signals.

Figure 5 shows a series of images acquired at different times during a typical MSX/UVISI occultation to illustrate the extinction of stellar light with altitude. The panels show composite SPIM spectral images together

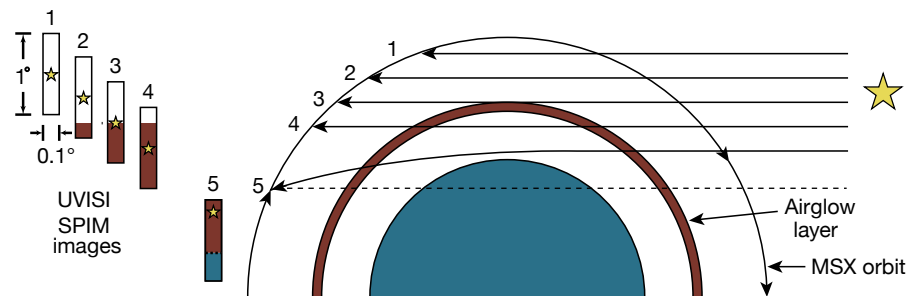


**Figure 4.** Schematic illustration of the MSX/UVISI stellar occultation geometry. The UVISI instrument is oriented so that the slit is vertical with respect to the atmosphere horizontal. The center of the slit is fixed on the star's inertial position throughout the occultation; therefore, the star itself can refract up to  $0.5^\circ$  before disappearing from the field of view. The  $1^\circ$  field of view in the vertical direction corresponds to  $\sim 60 \text{ km}$  at the limb. The superposition of the background airglow (magenta) and stellar signals once the line of sight has passed through the airglow layer is illustrated. The minimum height of the solid rays above Earth's surface (blue) reflects the apparent tangent point altitude, whereas the dashed line between the spacecraft and the star is an example of the geometric tangent point altitude, which can be negative. In the absence of refraction, the two quantities are equal. (Modified from a figure published in Ref. 29.)

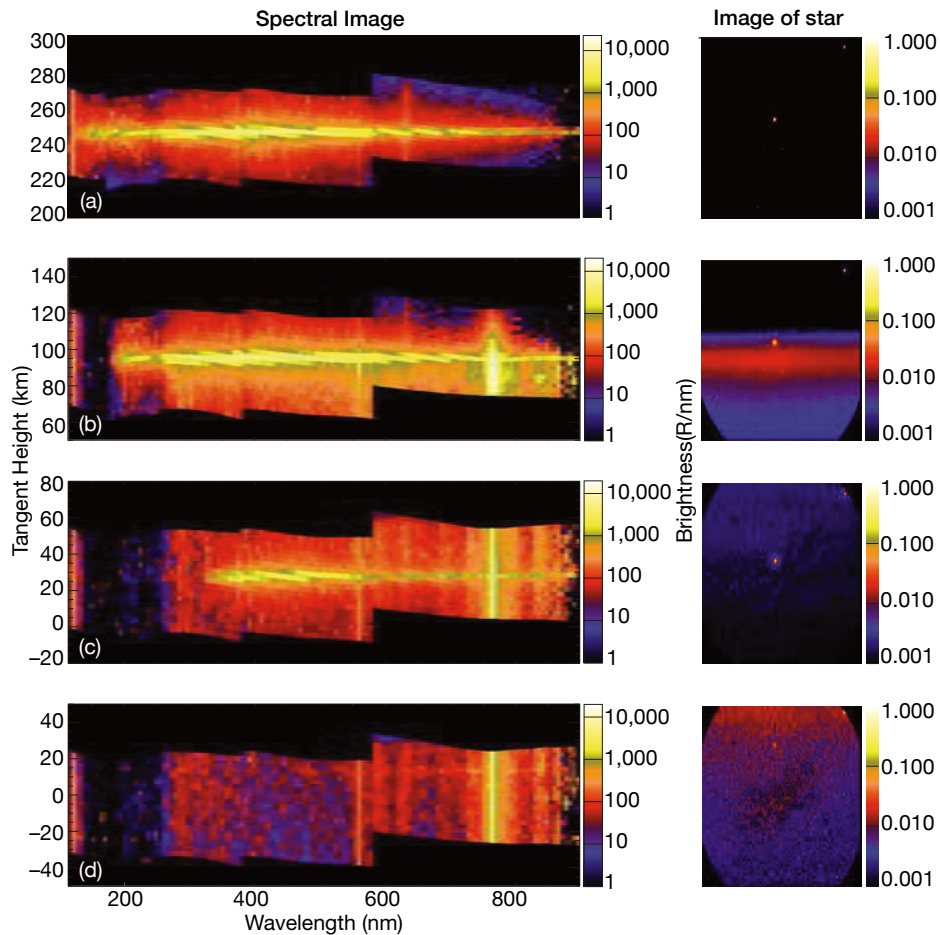


**Figure 5.** Series of UVISI images during a typical occultation event. The images on the left are from the spectrographic imagers and illustrate how the star’s spectrum (the bright horizontal line in the center of each image) is attenuated as a function of wavelength (left to right) and altitude (top to bottom). Note that the tangent height scale changes with each panel to be centered on the tangent height of the unrefracted star (i.e., its inertial position). Thus, the spectrum has moved “up” relative to the panel center in the final panel. Bright lines in the vertical direction are emissions from Earth’s atmosphere (i.e., the background airglow). The images on the right are from the IVN imager and show the position of the star corresponding to the spectrographic imager measurements on the left. Note that the star moves up away from the image center as refraction begins. The refraction angle is the angle between the center and measured positions. (Modified from a figure published in Ref. 29.)

with an IVN image acquired simultaneously. Scene brightness is represented by a color scale as a function of geometric tangent altitude (y axis) and wavelength (x axis) in the SPIM images. The star appears as a bright, narrow, horizontal band in the composite SPIM images because it is a point source emitting a continuous spectrum at all wavelengths, whereas the airglow signal covers an extended portion of the slit vertically owing to the diffuse nature of the airglow emission. The ragged horizontal edges of the SPIM images result from small, well-known misalignments of the five SPIM boresights plus corrections for optical aberrations when referencing the stellar signal at each wavelength to a common tan-

gent point altitude. Black areas in Fig. 5 correspond to altitudes outside the SPIM fields of view, and a decrease in the SPIM 5 sensitivity results in the weak signal at the longest wavelengths of the spectral range. The star of interest is the bright dot near the center of each IVN image.

The data in Fig. 5a correspond to a geometric tangent altitude of 245 km. There is essentially no atmospheric attenuation of the star at this altitude; however, several airglow emissions are visible in the spectrum [e.g., geocoronal H Lyman  $\alpha$  at 121.6 nm, nightglow O(<sup>1</sup>S) “green line” at 557.7 nm, and nightglow O(<sup>1</sup>D) “red lines” at 630.0 and 636.4 nm]. Spectra from such altitudes and

higher provide the unattenuated stellar  $I_0$  spectra needed to determine the atmospheric transmission.

In Fig. 5b, the line of sight has descended to a tangent altitude near 95 km. Complete attenuation of the star by  $O_2$  is evident in the Schumann-Runge continuum and bands shortward of 200 nm, whereas absorption by  $O_3$  in the Hartley/Huggins bands is just beginning near 255 nm. Emissions in Earth's mesospheric airglow layer are now visible [e.g.,  $O(^1S)$  "green line,"  $O_2$  Atmospheric (0-0) band at 762 nm, several OH Meinel bands in the near-IR]. The mesospheric emissions cover only the lower portion of the SPIM images because the upper part of the slit still views tangent heights above the mesospheric airglow emission layer. Even though the stellar signal short of 200 nm is gone, the H Lyman  $\alpha$  geocoronal line is still present owing to emission that originates above the tangent point and extends into the geocorona. From the geometry of Fig. 4, it can be seen that this "near-field" source also exists for the airglow layer, explaining why many of the airglow emissions are only moderately attenuated as the occultation progresses.

Figure 5c shows the image when the star has reached a geometric tangent height of 20 km. In the lower stratosphere, the  $O_3$  column density has increased to the point that absorption in the Hartley/Huggins bands is complete, whereas absorption in the relatively weak Chappuis band near 600 nm has now become significant. The star has also moved in the SPIM and IVN images, shifting slightly upward as a result of refraction. Note that the second star in the upper right corner of the IVN image is at a higher tangent height and has not yet been refracted. Finally, Rayleigh extinction, refractive attenuation, and scintillation effects are becoming increasingly important as evident in the overall reduction of the stellar signal.

In Fig. 5d the geometric tangent altitude of the star has descended to 0 km, but refraction is sufficient to keep the star visible above the horizon. The refractive shift of the star's position is evident not only in the IVN image but also in the SPIM data where the bright line delineating the stellar spectrum has moved upward relative to the slit center, which is fixed on the star's inertial position. The star's apparent tangent height is roughly 13 km as shown in SPIM 5. The stellar signal continues to weaken and is visible only at the longer wavelengths. Both Rayleigh scattering and refractive attenuation act to block the majority of the stellar signal at tropospheric altitudes. At the same time, the relative constancy of the "near-field" airglow emissions from panel to panel results in a comparable, or even brighter in the case of 762 nm, signal relative to the star. This ultimately results in a decreased signal-to-noise ratio in the wavelength channels of the stellar transmission spectra contaminated by airglow once the two signals are separated.

Each MSX/UVISI occultation consists of images such as those presented in Fig. 5. Before the atmospheric retrievals, the spectral images must be processed to remove a number of instrumental effects (e.g., changes in gain with altitude, dark subtraction), and the stellar spectra must be separated from the contaminating airglow background. Accomplishing this requires knowledge of the true stellar position in the SPIM images, which is calculated from the measured position of the star in the IVN images and known relationships in the relative alignments of the various instruments (thereby emphasizing the need to both know and maintain the relative co-alignment of the SPIMs and imager).

## Data Reduction and Analysis

The data reduction and analysis process, as implemented in separate subsystems on MSX, is shown schematically in Fig. 6 and can be broken down into four general steps. First, the IVN images are processed to determine the angles through which the star is refracted at all altitudes. This is accomplished using the known inertial position of the star and the measured positions of the star in the IVN images. Second, the SPIM spectra are processed to yield stellar transmission spectra. The most important aspect of this process is the separation of the stellar and airglow signals, which is possible owing to accurate measurement of the star's true position in the IVN and SPIM images, knowledge

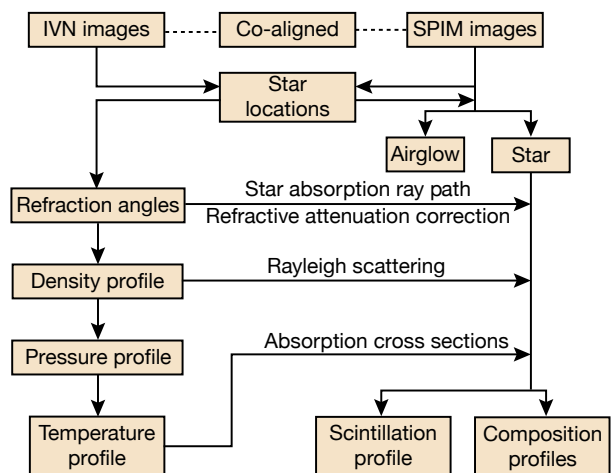


**Figure 6.** Schematic illustration of the combined stellar occultation data analysis process. Refraction information from the IVN images yields the bulk atmospheric properties of total density, pressure, and temperature. The SPIM images are processed to yield separate images of the star and background airglow, and the star images are then processed to yield the composition profiles for various species. The feedback of the bulk properties to the composition retrievals is indicated, and it is that feedback that allows the accurate determination of profiles in the lower atmosphere. (Reproduced from Ref. 29.)

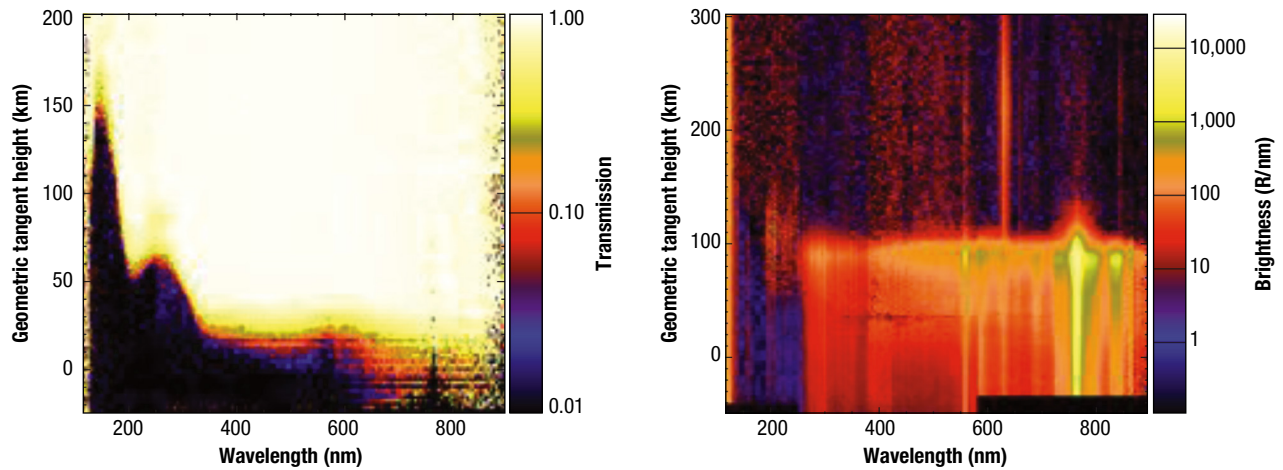


**Figure 7.** Stellar transmission (left) and airglow (right) spectra as a function of geometric tangent height and wavelength as observed by MSX/UVISI during the typical occultation event described in the text. Notice how the extinction edge of the starlight as a function of wavelength and tangent height matches the shape of the optical depths of the species in Fig. 3. Geometric tangent height refers to the tangent height of the unrefracted (i.e., inertial) stellar position, which is why the altitudes in the left panel still show stellar signal at negative altitudes (i.e., the star has gone below the horizon but refraction of the light allows signal to still reach the instruments). Note the different y axis scales in the two panels. (Reproduced from Ref. 29.)

of the spatial point spread functions of the five SPIMs, and the multiple sampling of the airglow data afforded by the spatial imaging capabilities of the SPIMs. Equally important in this process is the determination of the spectral uncertainties given that the stellar and airglow signals come from two different statistical distributions. Third, the bulk atmospheric properties (density, pressure, and temperature) are retrieved from the refraction angles using the technique developed by Vervack et al.<sup>31</sup> Finally, the O<sub>3</sub> profile is retrieved from the stellar transmission spectra using the technique described by DeMajistre and Yee.<sup>30</sup> It is important to note that the bulk properties from the refraction retrieval feed into the extinction retrieval, thereby allowing the proper temperature-dependent cross sections to be used, the actual refractive path to be calculated, and the Rayleigh scattering to be accurately accounted for when inferring the O<sub>3</sub> profile.

Although each step is executed separately, interconnections with the other steps exist and are critical to the combined occultation retrieval process. The position of the star in the high-angular-resolution (0.005°/pixel) IVN images not only yields refraction angles with sub-pixel accuracy but also provides the exact location of the star in the SPIM slits. Knowledge of the true position of the star in all the SPIM images is necessary in separating the airglow spectra from the stellar spectra, but this is especially the case once the star begins to move in the slit because of atmospheric refraction. The index of refraction profile retrieved directly from the observed refraction angles allows determination of the actual light path in the atmosphere for extinction calculations as well as the retrieval of the bulk atmosphere

density and temperature profiles. Finally, the retrieved bulk density profile constrains the amount of Rayleigh scattering inferred from the transmission spectra.

Figure 7 shows the separated transmission (left panel) and airglow volume emission (right panel) spectra for the typical occultation event. Absorption by O<sub>2</sub> and O<sub>3</sub> is clearly evident in the transmission spectra near 150 nm (thermospheric O<sub>2</sub>, Schumann-Runge continuum), 255 nm (mesospheric O<sub>3</sub>, Hartley band), and 600 nm (stratospheric/upper tropospheric O<sub>3</sub>, Chappuis band). Atmospheric scintillation causes the signal intensity to fluctuate below 40 km and results in the horizontal stripes in the atmospheric transmission. Because of atmospheric refraction, the star is observed even after the geometric line of sight has passed below the horizon (i.e., at negative geometric tangent heights). Abrupt changes in the noise characteristics and visual appearance of both the transmission and airglow spectra (e.g., at the juncture between SPIMs 3 and 4 near 380 nm) are caused by variations in wavelength sampling interval, instrument sensitivity, and resolution between the SPIMs. The peculiar structure near 760 nm is caused by difficulty in separating the stellar signal from the strong O<sub>2</sub> Atmospheric band emission.

Density profiles for the various species can be retrieved from transmission spectra such as those in Fig. 7. Above 60 km or so, extinction is effectively only due to absorption by O<sub>2</sub> and O<sub>3</sub>, there are no refraction effects, and the airglow contamination is relatively weak at the shorter wavelengths where extinction is present. Retrievals at these geometric tangent altitudes are thus relatively straightforward. Below 60 km, however, absorption from

several species is intertwined with Rayleigh and aerosol scattering, refraction begins to have significant effects, and airglow contamination is more evident. Although these factors complicate the retrievals, the composition and structure of the atmosphere can be determined by using the data from both the SPIMs and IVN.

### Examples of Retrieved Profiles

The results of the refraction and extinction retrievals for a typical occultation are presented in Fig. 8, with the temperature profile shown in the top panel and the  $O_3$  density profile shown in the bottom panel. Both MSX/UVISI profiles (red) are compared to profiles measured by sonde at the McMurdo, Antarctica, ground-based station (blue). McMurdo was nearly coincident in both time and space to the tangent point of the MSX/UVISI occultation. Note that the retrieved temperature profile does not extend all the way to the surface because the star refracted out of the imager field of view at apparent tangent altitudes between 6 and 7 km. In a follow-on instrument, direct tracking of the refracted star position or a larger field would capture the full range of motion in the refracted stellar position and enable temperature profile retrievals closer to the surface (most likely limited by cloud heights when clouds are present). Also shown in the bottom panel is the MSX/UVISI-determined  $O_3$  mixing ratio profile calculated using the density profile from the refraction retrieval. A significant advantage of the combined occultation technique is the direct calculation of mixing ratios using a simultaneously measured total density profile, providing a more accurate measure of mixing ratio than current methods that rely on model total density profiles.

Another significant point regarding Fig. 8 is that the temperature and  $O_3$  profiles are plotted versus both altitude and the retrieved pressure. This illustrates another important advantage of the combined extinctive/refractive technique: the pressure–altitude relationship is firmly known. The altitude grid used in the density profile retrievals is accurately established from the observation geometry, whereas the pressure profile is integrated directly from the measured total density profile and need not be inferred, as is commonly required in alternate methods. Such accurate knowledge of the pressure–altitude relationship increases the utility of the retrieved profiles in atmospheric models based on either pressure or altitude.

As with any measurements, there are several types of uncertainty that must be considered in the retrievals. Systematic uncertainty results from approximations made in the retrieval algorithms, imperfect knowledge of instrument characteristics, and the various assumptions incorporated into the retrievals. These are difficult to evaluate and often lead to biases when compared

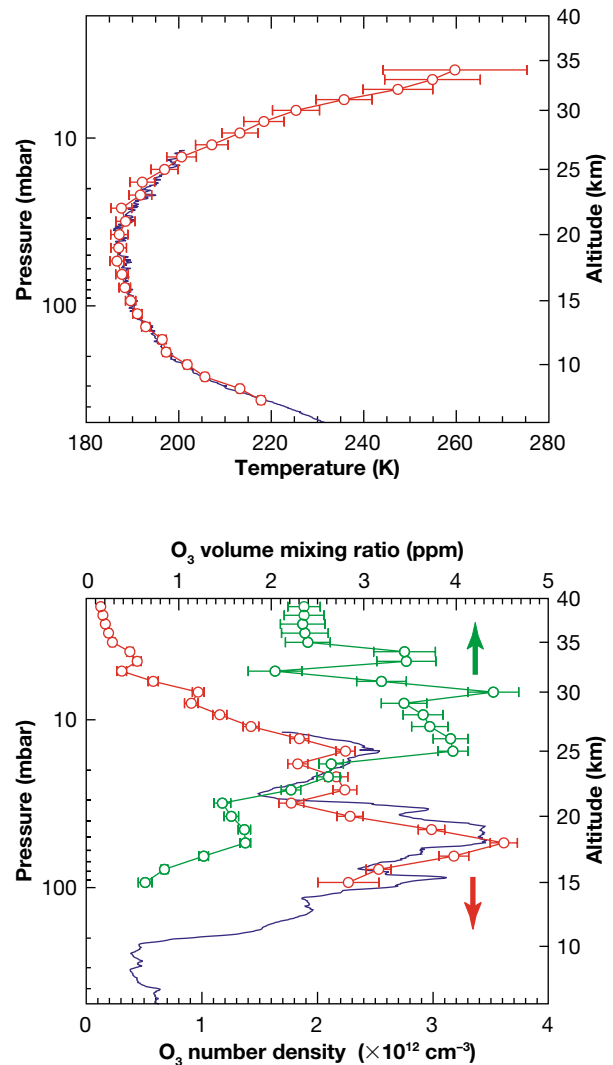


**Figure 8.** Comparison of temperature and  $O_3$  profiles retrieved from a typical MSX/UVISI stellar occultation event (red) to the profiles measured by sonde at the McMurdo, Antarctica, ground-based station (blue). The agreement is good at all altitudes, including some of the finer altitude structure in the density profile and particularly in light of the different spatial scales (i.e., *in situ* vs. a limb observation). The bottom panel also shows the MSX/UVISI  $O_3$  mixing ratio profile (green) calculated using the total density profile retrieved from the refraction measurements. Uncertainties ( $1-\sigma$ ) in the profile are shown in both panels as horizontal error bars; pressure/altitude uncertainties are on the order of the size of the symbols or smaller and are not visible at this scale.

to results from other methods. Statistical uncertainty results from the uncertainty in the measured transmission spectra and stellar positions as they propagate through the retrievals into the uncertainty of the derived profiles. For example, the finite precision of the MSX/UVISI total density and temperature profiles provided by the refraction measurements will have an

impact on the retrieved density profiles for the atmospheric species that can be properly accounted for (see the papers by DeMajistre and Yee<sup>30</sup> and Vervack et al.<sup>31</sup> for detailed discussions of the uncertainty sources and error analysis). As can be seen in the resulting statistical uncertainties in Fig. 8, however, the typical MSX/UVISI occultation event provides fairly accurate results despite the fact that MSX/UVISI was not optimized for these observations; an optimized instrument would do even better.

## SCIENTIFIC RESULTS

Between April 1996 and March 2000, MSX/UVISI observed roughly 200 stellar occultations. Owing to the scattered nature of the occultations in both time and location, general scientific studies have been limited to a few cases. Nevertheless, these cases have allowed for a quantitative demonstration of the capabilities of the combined extinctive and refractive stellar occultation technique.

### Wide-Ranging Altitude Coverage

During May 5–7, 1997, MSX/UVISI obtained 15 stellar occultations at a single latitude but spaced longitudinally. Shown in Fig. 9 are the weighted mean density profiles for O<sub>2</sub> and O<sub>3</sub> for this series of occultations. Although previous stellar occultation experiments have also yielded O<sub>2</sub> and O<sub>3</sub> profiles, the MSX/UVISI results are significant because of the large altitude range they cover.

Earlier measurements<sup>4,5</sup> of O<sub>2</sub> were limited to altitudes above 100 km or more. The MSX/UVISI results extend down to roughly 50 km owing to two factors. First, the wavelength coverage of the SPIMs extends to longer wavelengths with moderate spectral resolution, allowing use of the Schumann-Runge bands and the Herzberg continuum. Second, the SPIMs generate hyperspectral images that allow for the separation of the airglow signal from the stellar transmission. The spatial dimension of these images provides measurement of the airglow at altitudes above and below the line of sight to the star such that the airglow signal can be determined and removed from the pixels containing the stellar signal. Once the airglow signal is removed, the Schumann-Runge band and Herzberg continuum regions of the spectrum represent a purely stellar signal, and the O<sub>2</sub> profile can extend down into the mesosphere. Because the bulk density profile inferred from the refraction measurements can be converted to the equivalent O<sub>2</sub> density owing to the well-mixed nature of the lower atmosphere, the O<sub>2</sub> density profile can be effectively measured from 200 km or so down to the surface or cloud top heights with only a small gap between roughly 50 and 30 km.

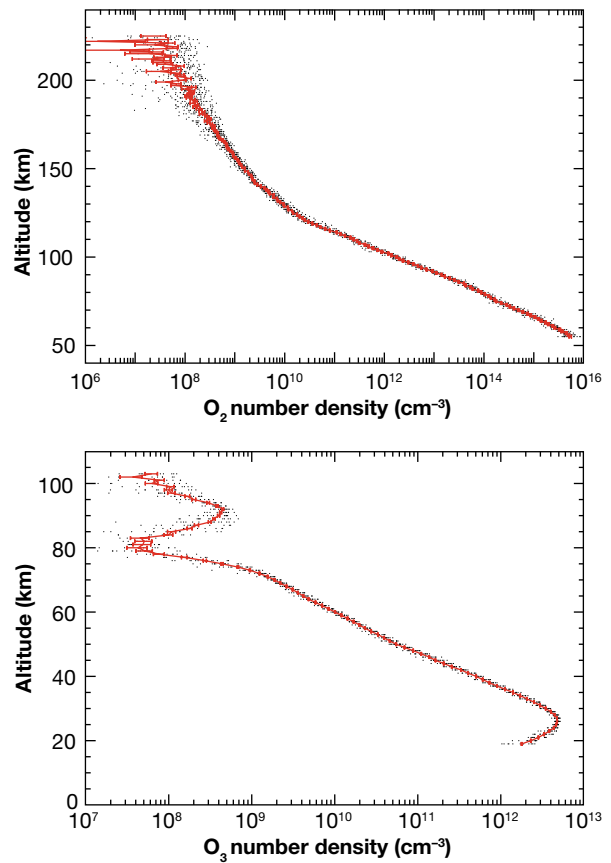


**Figure 9.** O<sub>2</sub> and O<sub>3</sub> profiles retrieved from a series of 15 MSX/UVISI stellar occultations. The dots represent the individual profiles, whereas the solid lines represent the weighted average profiles and their associated 1- $\sigma$  uncertainties. The change in slope of the O<sub>2</sub> profile near 120 km corresponds to the altitudes at which O<sub>2</sub> is no longer well mixed with the other atmospheric gases and begins to follow its own scale height. The O<sub>3</sub> profile clearly shows the main O<sub>3</sub> peak in the stratosphere near 25–30 km altitude as well as the secondary peak in the upper mesosphere/lower thermosphere near 90 km altitude. The ability to measure these two profiles from the lower atmosphere to the highest altitudes possible is significant owing to the chemical connections between the two species and their importance in understanding physical processes in Earth’s atmosphere.

Similar statements may be made regarding the O<sub>3</sub> profiles in Fig. 9. Previous measurements from stellar occultation experiments<sup>6</sup> only covered the altitudes down to roughly 60 km. The combination of the extended wavelength range and imaging capabilities of the UVISI SPIMs with the tracking capabilities of the MSX spacecraft allow for the removal of the airglow signal and measurement of the extinction in the Chappuis band of O<sub>3</sub> at visible wavelengths even when the star experienced significant refraction in the lower atmosphere. The true key to the success of these O<sub>3</sub> measurements, however, is the combination of both extinctive and refractive measurements because the bulk properties inferred from

the refraction data allow accurate treatment of Rayleigh scattering, the refractive attenuation of the starlight, and the change in the actual light path caused by refractive bending. Without the refraction measurements, using stellar occultations to measure lower atmospheric  $O_3$  would rely on a climatological model, thereby reducing the accuracy of the results.

## Intercomparison with Other Measurements

To investigate the quality of the retrieved MSX/UVISI  $O_3$  profiles and overall performance of the combined occultation method, a search for coincidences with ground-based facilities and measurements by space-based solar occultation instruments such as SAGE

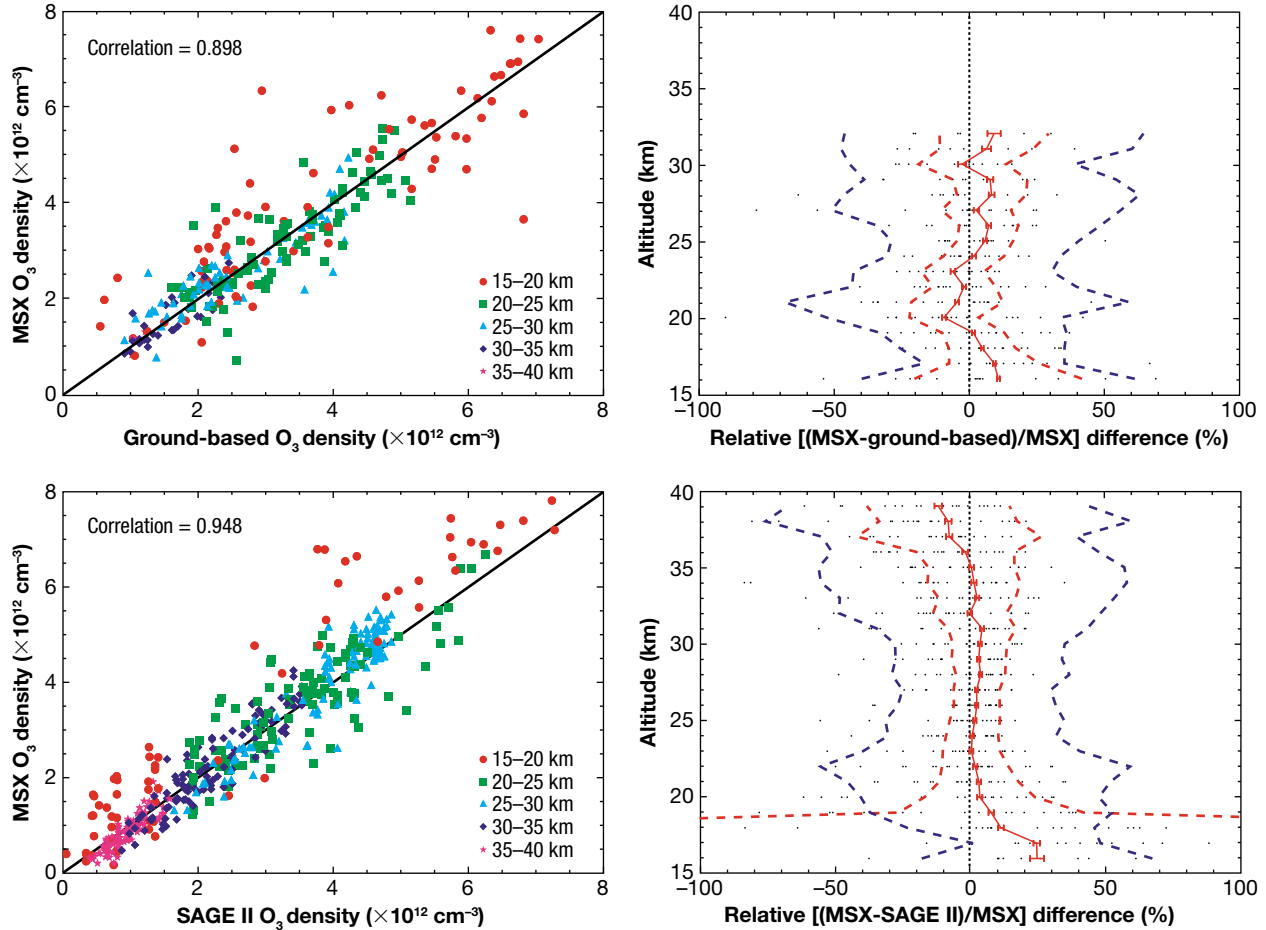


**Figure 10.** Comparison of MSX/UVISI-derived  $O_3$  values to ground-based sonde (top panels) and SAGE II data (bottom panels) for a number of occultations. The left panels show point-by-point comparisons of the absolute densities measured at the same altitudes (all ground-based and SAGE II data have been interpolated onto the 1-km altitude grid of the MSX/UVISI data), with the diagonal lines representing perfect agreement between MSX and the other data set. To illustrate the altitudes to which each point corresponds, the data have been color-coded according to the legends. For example, the dark green circles represent the points at altitudes between 15 and 20 km (i.e., 15, 16, 17, 18, 19, and 20). Note that there has not been any binning of the data over these ranges; the ranges are merely an indicator of the altitude region from which the data originate so that systematic biases at certain altitudes can be identified more easily. The right panels show the differences between the datasets as a function of altitude. At each altitude, the dots represent the point-by-point relative differences between MSX and the other data set. The solid red line is the weighted mean difference profile with the error bars on the solid red line representing the uncertainty in the weighted mean. The dashed red lines are the average  $3\sigma$  uncertainties inferred from the measurement uncertainties as propagated through the relative difference process of subtraction and division. In calculating these average uncertainties, both the uncertainties in the MSX/UVISI and the (properly interpolated) SAGE II data were used; however, for the ground-based comparisons, zero uncertainty in the comparison data was assumed because most of the ground-based data were provided without such information and we wished to treat all the ground-based data equally. The dashed blue lines are the  $3\sigma$  uncertainties calculated from the distribution of the relative difference points at each altitude without any weighting by the uncertainties in the relative differences. Thus, under the condition that the uncertainty estimates truly reflect the respective measurement uncertainties, the differences between the red and blue dashed lines are potentially a reflection of the geophysical variance among the various locations and times at which the measurements were made. (Reproduced from Ref. 33.)

(Stratospheric Aerosol and Gas Experiment) II was conducted. Search windows of  $\pm 5^\circ$  latitude,  $\pm 20^\circ$  longitude, and  $\pm 24$  h UTC were used. Although the longitude window may seem large, most coincidences occur from mid-latitudes to polar latitudes such that the separation in absolute distance is smaller than that from an equatorial standpoint. The majority of the coincidences are well within the allowed window regardless, and similar windows have been used in validating SAGE II data.<sup>32</sup> These search parameters yielded 17 ground-based and 20 SAGE II coincidences.

When comparing measurements from different techniques, the context of the measurement scenarios must be factored in. Time, altitude, and instrument resolutions vary and affect the comparisons. Horizontal resolution differs greatly between ground-based and space-based measurements, with the former being fairly localized in extent whereas the latter can have a horizontal resolution of several hundred kilometers across the limb. The choice of absorption and scattering cross sections is another potential source of differences, due to both absolute calibration issues in the laboratory measurements and the temperature dependence of these data (highlighting the need for an accurate temperature profile as provided by the combined technique). Systematic comparisons of various measurement techniques are thus a common means of assessing the differences and similarities.

As can be seen in Fig. 10, comparisons between MSX/UVISI and “ground-based” (primarily sondes, top panels)  $O_3$  density measurements are excellent. Although there is some scatter in the  $45^\circ$  plot (top left panel), there is no clearly evident systematic bias. Further evidence for good agreement is provided by the weighted mean difference profile in the top right panel of Fig. 10, which is more or less centered on the

zero line. Comparisons to space-based observations by SAGE II (bottom panels), one of the standards in  $O_3$  measurements, are also strikingly good. Near the  $O_3$  peak between 20 and 36 km (retrievals are generally most accurate near the density peaks), the differences are better than 5%, although a slight systematic bias is evident in that the MSX/UVISI values are generally larger than the SAGE II values (i.e., positive residuals in the weighted mean). At higher altitudes, there is a systematic bias toward negative differences, but the agreement is still better than 10%. A larger systematic difference is present at low altitudes, with the bias toward positive differences. The source of these high- and low-altitude biases may be related, in part, to the use of the Sun as the source for the SAGE II measurements. Because the Sun subtends a finite range of altitudes in the atmosphere, it is difficult to disentangle the absorption at a specific altitude. In contrast, the stars used by MSX/UVISI are point sources and provide better altitude resolution. The rapid increase in the uncertainty of the SAGE II differences at low altitudes is due to highly uncertain retrievals from the SAGE II data, which suffer at the lowest altitudes once the line of sight in their observations falls below the  $O_3$  peak density. SAGE II uncertainties at the lowest altitudes can approach the level of the measurements themselves, whereas the uncertainty in the combined technique results is significantly smaller (see Fig. 8). Issues with knowledge of the refractive state of the atmosphere and the total density and temperature, which are not measured simultaneously by SAGE II (their results generally incorporate climatological model profiles), likely play into the differences at the lowest altitudes as well.

A similar comparison was made between the retrieved MSX/UVISI temperature profiles and profiles

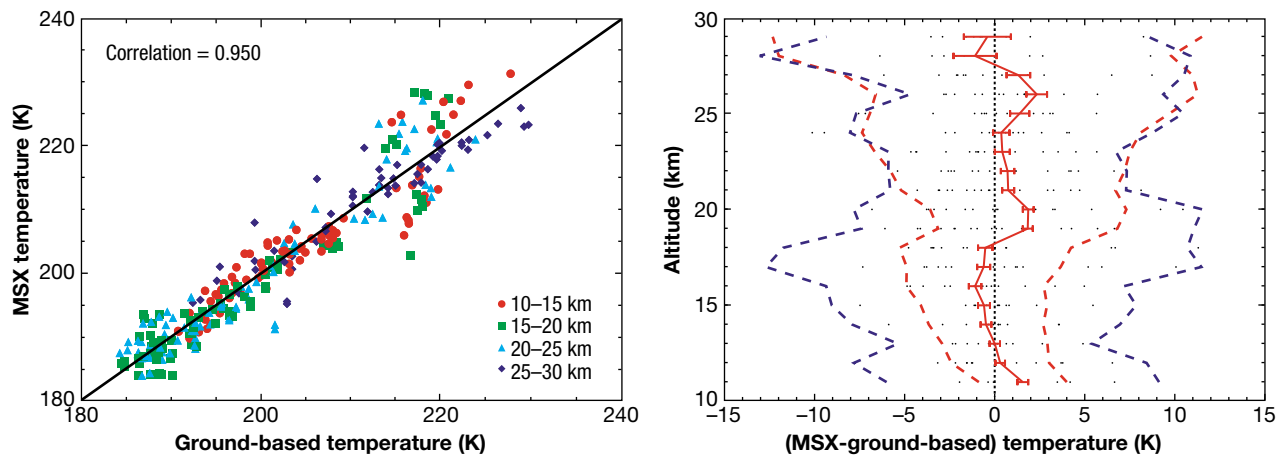


**Figure 11.** Comparison of MSX/UVISI-derived temperature values to ground-based sonde data. The panels are similar to those in Fig. 10 with the exception that the right panel shows absolute rather than relative differences. The solid red, dashed red, and dashed blue lines represent the equivalent quantities as in the relative  $O_3$  difference plots of Fig. 10. (Reproduced from Ref. 33.)

from ground-based measurements (Fig. 11). As with the  $O_3$  comparisons, the MSX/UVISI data compare well with the ground-based temperature data, particularly given the *in situ* nature of the ground-based data compared to the wider horizontal scale of the occultations. The larger scatter around 220 K in the  $45^\circ$  plot (left panel) is primarily caused by three temperature profiles obtained at the Lauder, New Zealand, monitoring station. Because the MSX/UVISI data agree well with other Lauder profiles, this subset of poor agreement is somewhat puzzling, but they are included to avoid systematic biasing of the intercomparison. It may be noteworthy that stars for two of these MSX/UVISI occultations were particularly dim, of a poor spectral type for UV/visible occultations, or both. The increased scatter at higher altitudes is likely due in part to large uncertainties in the sonde data near the maximum altitudes of the balloons.

The absolute temperature difference plot in the right panel of Fig. 11 shows excellent agreement between the MSX/UVISI and ground-based data. The majority of the absolute differences are less than 5 K at all altitudes, and the differences shown by the weighted mean profile are better than 2 K. A slight bias to larger

MSX/UVISI values is indicated at most altitudes above 20 km, which is possibly related to two causes: refraction angle uncertainties and sonde capabilities. The refraction angle uncertainties approach the size of the refraction angles themselves at these altitudes. Vervack et al.<sup>31</sup> noted this as a reasonable indicator of the limits of the visible-light refraction angle approach, but this is well captured in the statistical uncertainty of the MSX/UVISI temperature retrievals and should not introduce a significant systematic bias. Also at these altitudes, the measurement capabilities of the sondes begin to reach their limits, and the measurements are correspondingly less accurate, which may introduce a systematic trend if they tend to underestimate the temperatures. Over the altitude range where the observations from both data sets are best known, however, the agreement is quite good.

The results in Figs. 10 and 11 show that the combined occultation technique compares well with established, routine methods and instruments used to measure  $O_3$  and temperature and that it represents a highly valuable, complementary means of monitoring atmospheric  $O_3$ . Further details on the intercomparison study may be found in the paper by Vervack et al.<sup>33</sup>

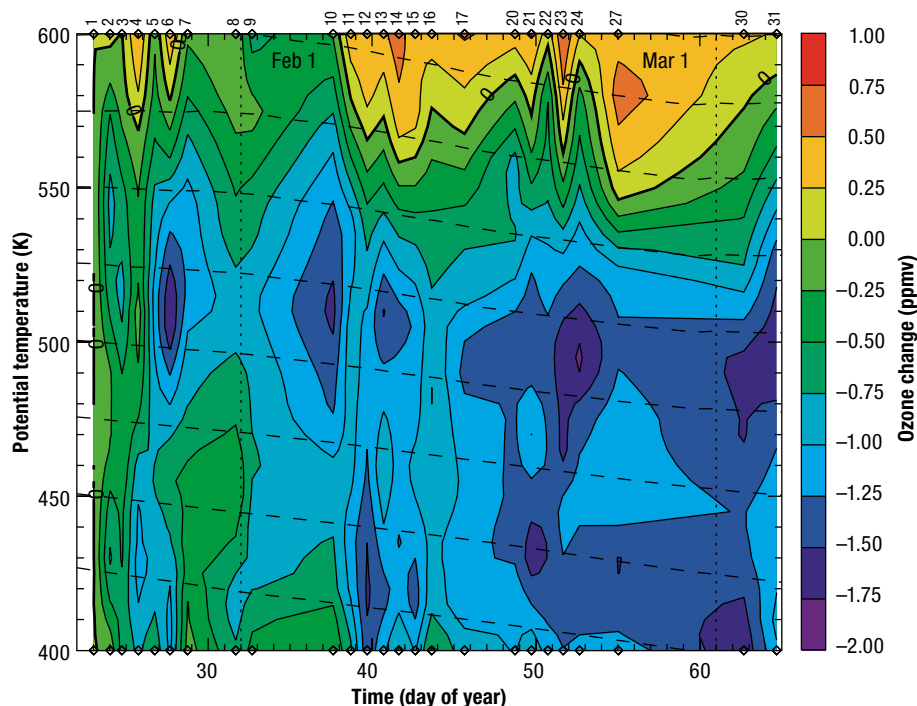


**Figure 12.** Changes in the  $O_3$  mixing ratio in the lower stratosphere within the Arctic polar vortex as measured by MSX/UVISI during the SOLVE campaign. Altitude is represented in terms of potential temperature. The times of the MSX/UVISI stellar occultations are denoted by diamonds along the upper and lower abscissas and identified by profile number. Vertical dotted lines indicate February 1 and March 1. The dashed lines denote the ensemble average diabatic descent of air parcels within the vortex passing through the tangent points of the MSX/UVISI observations. (Reproduced from Ref. 36.)

### The SOLVE Campaign

We used MSX to demonstrate the scientific utility of this measurement technique during the SAGE III Ozone Loss and Validation Experiment (SOLVE) campaign. During wintertime over the poles, a dynamically isolated, continental-scale vortex forms in the stratosphere. Within this vortex, more popularly known as the “ozone hole,” air cools radiatively and sinks. Halogen species become chemically activated on the surfaces of polar stratospheric cloud particulates and catalytically destroy O<sub>3</sub> with the return of sunlight in the late winter/early spring. Between November 1999 and March 2000, the SOLVE campaign was conducted simultaneously with the Third European Stratospheric Experiment on Ozone 2000 (THESEO 2000), based in Kiruna, Sweden (68°N, 20°E). The campaign was focused on coordinated observations from aircraft-, balloon-, ground-, and space-based instruments with the goal of assessing quantitatively the rate of high-latitude stratospheric O<sub>3</sub> loss in order to gain a better understanding of the processes controlling the loss of stratospheric O<sub>3</sub> at mid- to high northern latitudes.

There were 31 MSX/UVISI stellar occultation observations conducted during the SOLVE campaign, from January 23 through March 4, 2000. Twenty-five of these occultations occurred within the Arctic vortex, and the results of the O<sub>3</sub> retrievals in the lower stratosphere for these in-vortex profiles are shown in Fig. 12 as a function of potential temperature (roughly corresponding to altitude). Rather than absolute mixing ratios, this figure shows the change in O<sub>3</sub> mixing ratio as a function of time (measurement times are indicated at the top and bottom of the figure). The extent of subsidence within the vortex is indicated by the ensemble average descent rates for air parcels (averaged over 25-K intervals and indicated by the dashed lines); an overall trend in O<sub>3</sub> loss is observed, particularly below 500 K.

Within the lower stratosphere, O<sub>3</sub> mixing ratios increase with altitude; any subsidence will thus tend to increase the observed O<sub>3</sub> mixing ratios with time. Such increases may partly mask the observable effects of actual chemical O<sub>3</sub> destruction. Therefore, to make quantitative inferences about chemical O<sub>3</sub> loss, the dynamical effects within the vortex must be accounted for in O<sub>3</sub> retrievals such as those in Fig. 12. The Goddard Space Flight Center trajectory model<sup>34</sup> was used to conduct diabatic trajectory calculations to follow individual air parcels from each occultation profile forward to March 4, the date of the final occultation. Each retrieved O<sub>3</sub> profile was interpolated onto diabatic surfaces intersecting a 5-K grid using pairs of adjacent trajectories. The grid was established using the potential temperatures on March 4 from the trajectory models. The results on three such surfaces, intersecting the 575-, 500-, and 425-K potential temperature surfaces on March 4, are shown in Fig. 13. Each plot represents cross sections par-

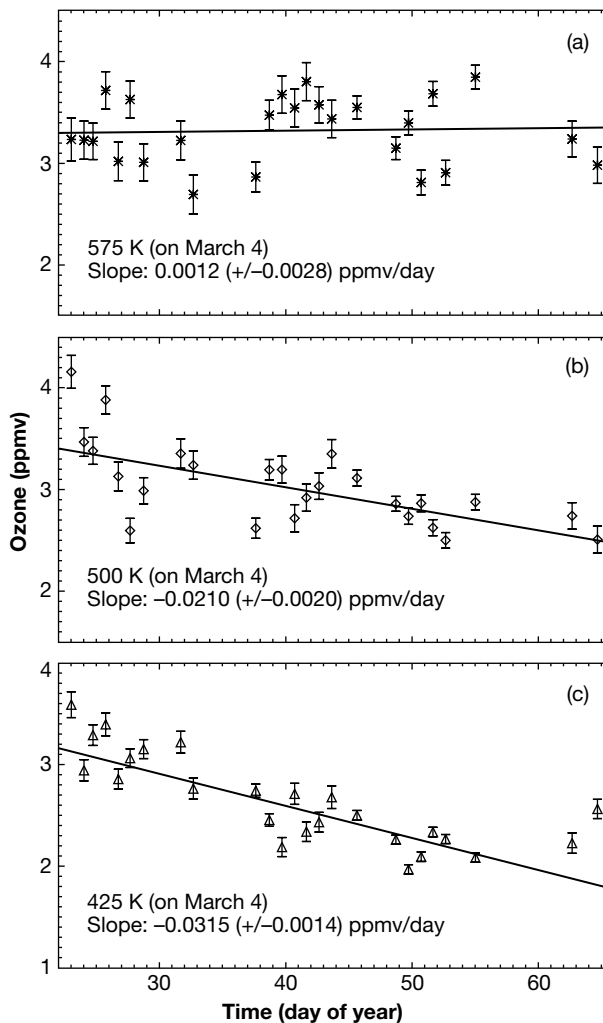


**Figure 13.** Photochemical O<sub>3</sub> loss within the polar vortex along three particular diabatic surfaces as observed by MSX/UVISI during the SOLVE campaign. The error bars denote the 1-σ uncertainties of the occultation measurements and retrieval and do not include the uncertainty in the trajectory calculations. The average daily loss rates for the period (i.e., the absolute values of the slopes resulting from weighted linear regressions through the observations on each surface) are also shown, along with the uncertainties in the fits. (Reproduced from Ref. 36.)

allel (on average) to the diabatic descent curves of Fig. 12 (dashed lines). The slopes of the fits to the measurement points in Fig. 13 correspond to the average daily O<sub>3</sub> loss rates at each level during the SOLVE campaign period. Although little net change is observed in the O<sub>3</sub> mixing ratio at 575 K, increasing loss with decreasing altitude is observed in the trend to lower potential temperatures, with a maximum loss near 425 K. A maximum O<sub>3</sub> loss of about 1 ppmv at 400–500 K (~16–21 km) was determined and corresponds to an average loss rate of ~0.024 ppmv/d, in agreement with other SOLVE determinations of O<sub>3</sub> loss.<sup>35</sup> Further details on the SOLVE study may be found in the paper by Swartz et al.<sup>36</sup>

## FUTURE CHALLENGES

Although MSX/UVISI was not optimized for stellar occultations, the MSX experiments successfully reduced to practice the techniques outlined in this article. MSX provided a valuable opportunity to test the combined extinctive and refractive stellar occultation technique through many observations and validated the technique. Even in this nonoptimized state, the MSX/UVISI data have yielded atmospheric profiles that compare well with established ground-based and space-based measurements.<sup>33</sup> In particular, the excellent agreement between the ground-based data and the MSX/UVISI results, both in O<sub>3</sub> and temperature, provides strong evidence that an instrument specifically designed for implementation of the combined occultation technique can provide O<sub>3</sub> profiles down into the troposphere, with accuracy at least comparable to that of current techniques but offering the prospect of global measurements covering a greater range of locations and times. Ground-based data are limited to a few locations on Earth, and instruments such as SAGE II, which uses the Sun as an occultation source, are limited to the terminator region and cannot probe the atmosphere globally on short timescales; a stellar occultation method does not suffer from these limitations. The combined technique is thus a viable method for probing Earth's lower atmosphere for both composition and bulk properties and has the potential to become a powerful new observational technique for global monitoring of lower atmospheric O<sub>3</sub> and other trace gas species.

Daily, global monitoring of the atmosphere via stellar occultations has been implemented on spacecraft platforms that flew after MSX [e.g., by the GOMOS (Global Ozone Monitoring by Occultation of Stars) instru-

ment on Envisat-1<sup>37</sup>]. However, these instruments were not designed to exploit the full potential of the stellar occultation technique and in particular were not able to probe the important lower atmosphere accurately. The MSX/UVISI experiments have demonstrated that the combined technique can provide the global measurements needed by the scientific and policy-making communities, with accuracy equivalent to or with an optimized instrument better than the current state of the art. Thus, an optimally designed stellar occultation instrument that packages all the necessary elements in a single box is required to take this new technique to the next level.

Our group at APL has addressed this need. Through a NASA Instrument Incubator Program project, the design of an optimized instrument, known as STARS (STellar Absorption and Refraction Sensor) has been conducted.<sup>38</sup> The goals of this project were three-fold. The first goal was to perform a trade-off analysis between measurement capabilities and instrument requirements to ensure that the final design met the desired measurement objectives as shown in Fig. 1. The second goal was to design an instrument independently capable of performing the stringent tracking requirements necessary for the combined stellar occultation technique, thereby allowing its flight on any number of spacecraft platforms offering only modest tracking capabilities. The third and final goal was to test the critical tracking subsystem components in the laboratory (see Fig. 14) in order to increase the technology readiness levels of these elements to flight proposal status. Unfortunately, despite the success of the STARS project in achieving all its goals, shifting priorities in Earth science led to a lack of flight opportunities.

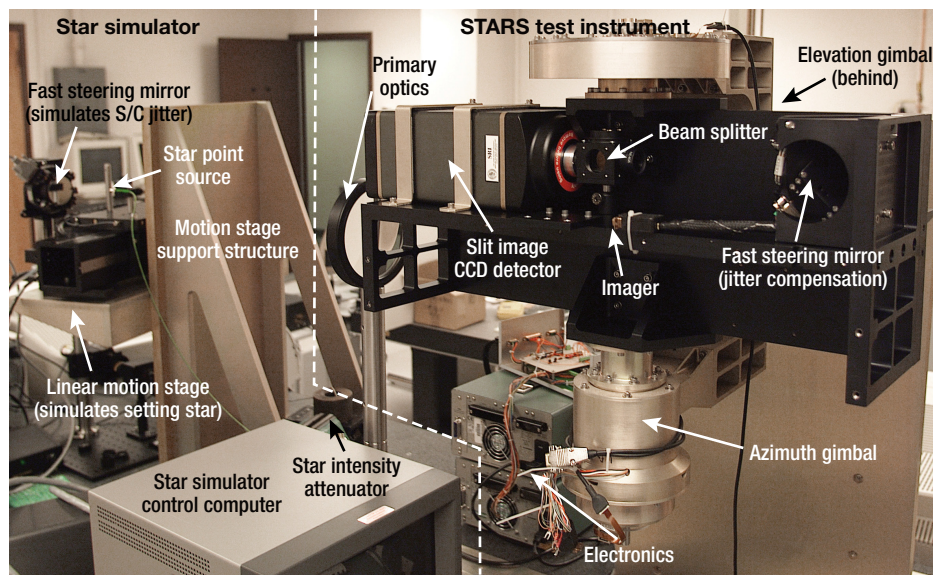


**Figure 14.** Laboratory setup for testing of the tracking capabilities of the STARS instrument. (Modified from a figure published in Ref. 38.)

More recently, a renewed emphasis on Earth science has emerged from NASA in the form of the Earth Venture line of missions. These small to medium, low-cost missions are ideal for stellar occultation measurements; however, the STARS instrument is too large for these missions. The current challenge, therefore, is to redesign the STARS system for implementation on the next generation of these smaller satellites. Enabling technologies in the form of uncooled IR detectors, advanced microprocessors and focal plane elements, and miniaturized electronics need to be leveraged to reduce the instrument size and enable this powerful remote sensing technique that has the advantage of both low-cost and low-resource requirements.

From the proof-of-concept demonstrations with MSX/UVISI to the breadboard optimization of STARS, APL is positioned on the forefront of this exciting new method for remotely sensing Earth's lower atmosphere and beyond.

**ACKNOWLEDGMENTS:** We thank Frank Morgan, James Carbary, Gerry Romick, Danny Morrison, Steve Lloyd, Phil DeCola, Don Anderson, and Kris Kumar for their part in fostering the combined occultation technique. We acknowledge the MSX team at APL for their roles in the operation, scheduling, data processing, and calibration of the MSX spacecraft and instruments, as well as the efforts of the STARS instrument development team. The ground-based data were obtained via FTP from the World Ozone and Ultraviolet Data Centre provided by the Meteorological Service of Canada, Environment Canada. The SAGE II data (Version 6.0) were obtained by CD from the NASA Langley Research Center Atmospheric Sciences Data Center. We thank all the investigators involved for making these data available to the scientific community. Funding for the data acquisition and operation of the satellite has been through the DoD's Ballistic Missile Defense Organization. The MSX/UVISI stellar occultation analysis was supported by internal APL basic research funding and NASA Grants NAG5-7552, NAG5-9988, and NAG-12270 to APL. The development of the STARS instrument was supported by NASA Contract NAS5-97271 to APL. The ideas summarized in this paper are captured in greater detail in Refs. 29–31, 33, and 38.

**REFERENCES**

<sup>1</sup>Graedel, T. E., and Crutzen, P. J., "The Changing Atmosphere," in *Managing Planet Earth, Readings from Scientific American*, Freeman, New York (1990).  
<sup>2</sup>Houghton, J. T., Ding Y., Griggs, D. J., Noguer, M., van der Linden, P. J., et al. (eds.), *Climate Change 2001: The Scientific Basis*, Intergovernmental Panel on Climate Change, Cambridge University Press, New York (2001).  
<sup>3</sup>Hays, P. B., and Roble, R. G., "Stellar Spectra and Atmospheric Composition," *J. Atmos. Sci.* **25**(6), 1141–1153 (1968).  
<sup>4</sup>Hays, P. B., Roble, R. G., and Shah, A. N., "Terrestrial Atmospheric Composition from Stellar Occultations," *Science* **176**(4036), 793–794 (1972).

<sup>5</sup>Hays, P. B., and Roble, R. G., "Stellar Occultation Measurements of Molecular Oxygen in the Lower Thermosphere," *Planet. Space Sci.* **21**(3), 339–348 (1973).  
<sup>6</sup>Hays, P. B., and Roble, R. G., "Observation of Mesospheric Ozone at Low Latitudes," *Planet. Space Sci.* **21**(2), 273–279 (1973).  
<sup>7</sup>Riegler, G. R., Atreya, S. K., Donahue, T. M., Liu, S. C., Wasser, B., and Drake, J. F., "UV Stellar Occultation Measurements of Nighttime Equatorial Ozone," *Geophys. Res. Lett.* **4**(4), 145–148 (1977).  
<sup>8</sup>Atreya, S. K., "Measurement of Minor Species (H<sub>2</sub>, Cl, O<sub>3</sub>, NO) in the Earth's Atmosphere by the Occultation Technique," *Adv. Space Res.* **1**(9), 127–141 (1981).  
<sup>9</sup>Roscoe, H. K., Freshwater, R. A., Wolfenden, R., Jones, R. L., Fish, D. J., et al., "Using Stars for Remote-Sensing of the Earth's Stratosphere," *Applied Optics* **33**(30), 7126–7131 (1994).  
<sup>10</sup>Renard, J.-B., Pirre, M., Robert, C., Moreau, G., Huguenin, D., and Russell, J. M. III, "Nocturnal Vertical Distribution of Stratospheric O<sub>3</sub>, NO<sub>2</sub> and NO<sub>3</sub> from Balloon Measurements," *J. Geophys. Res.* **101**(D22), 28,793–28,804 (1996).  
<sup>11</sup>Broadfoot, A. L., Sandel, B. R., Shemansky, D. E., Atreya, S. K., Donahue, T. M., et al., "Ultraviolet Spectrometer Experiment for the Voyager Mission," *Space Sci. Rev.* **21**(2), 183–205 (1977).  
<sup>12</sup>Smith, G. R., and Hunten, D. M., "Study of Planetary Atmospheres by Absorptive Occultations," *Rev. Geophys.* **28**(2), 117–143 (1990).  
<sup>13</sup>Pannekoek, A., "Über die Erscheinungen, Welche bei Einer Sternbedeckung Durch Einen Planeten Auftreten," *Astron. Nachr.* **164**(1), 5–10 (1904).  
<sup>14</sup>Baum, W. A., and Code, A. D., "A Photometric Observation of the Occultation of  $\sigma$  Arietis by Jupiter," *Astron. J.* **58**(1208), 108–112 (1953).  
<sup>15</sup>Wasserman, L. H., and Veverka, J., "On the Reduction of Occultation Light Curves," *Icarus* **20**(3), 322–345 (1973).  
<sup>16</sup>French, R. G., and Lovelace, R. V. E., "Strong Turbulence and Atmospheric Waves in Stellar Occultations," *Icarus* **56**(1), 122–146 (1983).  
<sup>17</sup>Elliot, J. L., Dunham, E. W., Bosh, A. S., Slivan, S. M., Young, L. A., et al., "Pluto's Atmosphere," *Icarus* **77**(1), 148–170 (1989).  
<sup>18</sup>Hubbard, W. B., Sicardy, B., Miles, R., Hollis, A. J., Forrest, R. W., et al., "The Occultation of 28 Sgr by Titan," *Astron. Astrophys.* **269**(1–2), 541–563 (1993).  
<sup>19</sup>Hunten, D. M., and Veverka, J., "Stellar and Spacecraft Occultations by Jupiter: A critical Review of Derived Temperature Profiles," in *Jupiter*, T. Gehrels (ed.), University of Arizona Press, Tucson, pp. 247–283 (1976).  
<sup>20</sup>Elliot, J. L., "Stellar Occultation Studies of the Solar System," *Ann. Rev. Astron. Astrophys.* **17**, 445–475 (1979).  
<sup>21</sup>Mill, J. D., O'Neil, R. R., Price, S., Romick, G. J., Uy, O. M., et al., "Midcourse Space Experiment: Introduction to the Spacecraft, Instruments, and Scientific Objectives," *J. Spacecr. Roc.* **31**(5), 900–907 (1994).  
<sup>22</sup>Carbary, J. F., Darlington, E. H., Harris, T. J., McEvaddy, P. J., Mayr, M. J., et al., "Ultraviolet and Visible Imaging and Spectrographic Imaging Instrument," *Appl. Opt.* **33**(19), 4201–4213 (1994).  
<sup>23</sup>Paxton, L. J., Meng, C.-L., Anderson, D. E., and Romick, G. J., "MSX—A Multiuse Space Experiment," *Johns Hopkins APL Tech. Dig.* **17**(1), 19–34 (1996).  
<sup>24</sup>Jones, L. M., Fischbach, F. F., and Peterson, J. W., "Satellite Measurements of Atmospheric Structure by Refraction," *Planet. Space Sci.* **9**(6), 351–352 (1962).  
<sup>25</sup>Grechko, G. M., Gurvich, A. S., Lyakhov, V. A., Savchenko, S. A., and Sokolovskiy, S. V., "Results of an Investigation of Refraction during the Third Expedition on the Salyut-6 Orbiter" (English translation), *Izv. Russ. Acad. Sci. Atmos. Oceanic Phys.* **17**, 835–841 (1981).  
<sup>26</sup>White, R. L., Tanner, W. E., and Polidan, R. S., "Star Line-of-Sight Refraction Observations from the Orbiting Astronomical Observatory Copernicus and Deduction of Stratospheric Structure in the Tropical Region," *J. Geophys. Res.* **88**(C13), 8535–8542 (1983).  
<sup>27</sup>Ware, R., Exner, M., Feng, D., Gorbunov, M., Hardy, K., et al., "GPS Sounding of the Atmosphere from Low Earth Orbit: Preliminary Results," *Bull. Amer. Meteor. Soc.* **77**(1), 19–40 (1996).  
<sup>28</sup>Kursinski, E. R., Hajj, G. A., Bertiger, W. I., Leroy, S. S., Meehan, T. K., et al., "Initial Results of Radio Occultation Observations of Earth's Atmosphere Using the Global Positioning System," *Science* **271**(5252), 1107–1110 (1996).

- <sup>29</sup>Yee, J.-H., Vervack, R. J. Jr., DeMajistre, R., Morgan, F., Carbary, J. F., et al., "Atmospheric Remote Sensing Using a Combined Extinctive and Refractive Stellar Occultation Technique: 1. Overview and Proof-of-Concept Observations," *J. Geophys. Res.* **107**(D14), ACH 15-1–ACH 15-13 (2002).
- <sup>30</sup>DeMajistre, R., and Yee, J.-H., "Atmospheric Remote Sensing Using a Combined Extinctive and Refractive Stellar Occultation Technique: 2. Inversion Method for Extinction Measurements," *J. Geophys. Res.* **107**(D15), ACH 6-1–ACH 6-18 (2002).
- <sup>31</sup>Vervack, R. J. Jr., Yee, J.-H., Carbary, J. F., and Morgan, F., "Atmospheric Remote Sensing Using a Combined Extinctive and Refractive Stellar Occultation Technique: 3. Inversion Method for Refraction Measurements," *J. Geophys. Res.* **107**(D15), ACH 7-1–ACH 7-19 (2002).
- <sup>32</sup>Veiga, R. E., Cunnold, D. M., Chu, W. P., and McCormick, M. P., "Stratospheric Aerosol and Gas Experiments I and II Comparisons with Ozonesondes," *J. Geophys. Res.* **100**(D5), 9073–9090 (1995).
- <sup>33</sup>Vervack, R. J. Jr., Yee, J.-H., DeMajistre, R., and Swartz, W. H., "Intercomparison of MSX/UVISI-Derived Ozone and Temperature Profiles with Ground-Based, SAGE II, HALOE, and POAM III Data," *J. Geophys. Res.* **108**(D22), ACH 2-1–ACH 2-19 (2003).
- <sup>34</sup>Schoeberl, M. R., and Newman, P. A., "A Multiple-Level Trajectory Analysis of Vortex Filaments," *J. Geophys. Res.* **100**(D12), 25,801–25,815 (1995).
- <sup>35</sup>Newman, P. A., Harris, N. R. P., Adriani, A., Amanatidis, G. T., Anderson, J. G., et al., "An Overview of the SOLVE-THESEO 2000 Campaign," *J. Geophys. Res.* **107**(D20), SOL 1-1–SOL 1-26 (2002).
- <sup>36</sup>Swartz, W. H., Yee, J.-H., Vervack, R. J. Jr., Lloyd, S. A., and Newman, P. A., "Photochemical Ozone Loss in the Arctic as Determined by MSX/UVISI Stellar Occultation Observations during the 1999/2000 Winter," *J. Geophys. Res.* **107**(D20), SOL 39-1–SOL 39-10 (2002).
- <sup>37</sup>Bertaux, J. L., Mégie, G., Widemann, T., Chassefière, E., Pellinen, R., et al., "Monitoring of Ozone Trend by Stellar Occultations: The GOMOS Instrument," *Adv. Space Res.* **11**(3), 237–242 (1991).
- <sup>38</sup>Yee, J.-H., Morrison, D., Murphy, G. A., Morgan, M. F. III, Humm, D. C., et al., "STARS: the Stellar Absorption and Refraction Sensor," in *Optical Spectroscopic Techniques, Remote Sensing, and Instrumentation for Atmospheric and Space Research IV*, Proc. SPIE Vol. 4485, A. M. Larar and M. G. Mlynczak (eds.), SPIE, Bellingham, WA, pp. 51–59 (2002).

# The Authors

**Ronald J. Vervack Jr.** was the lead on the refraction observation analysis for the MSX/UVISI stellar occultation experiments and also lead on the intercomparisons to measurements made by other spacecraft and ground-based facilities. He is a member of the APL Senior Professional Staff in the Space Exploration Sector's Geospace and Earth Science (SRG) Group. **Jeng-Hwa (Sam) Yee** is Branch Scientist for Earth Science in the Space Exploration Sector and was responsible for the overall conduct and analysis of the MSX/UVISI stellar occultations. **William H. Swartz** is Assistant Group Supervisor of the Space Exploration Sector's SRG Group and was the lead on the collaborative effort during the international SOLVE campaign. **Robert DeMajistre** is Assistant Group Supervisor of the Space Exploration Sector's Science Applications (SIS) Group and was the lead on the extinction observation analysis for the MSX/UVISI stellar occultation experiments. **Larry J. Paxton** is the SRG Group Supervisor and was instrumental in identifying the scientific potential of MSX/UVISI for Earth remote sensing. For further information on the work reported here, contact Ron Vervack. His e-mail address is [ron.vervack@jhuapl.edu](mailto:ron.vervack@jhuapl.edu).

The Johns Hopkins APL Technical Digest can be accessed electronically at [www.jhuapl.edu/techdigest](http://www.jhuapl.edu/techdigest).